

Single-walled carbon nanotube membranes for optical applications in the extreme ultraviolet range

V. M. Gubarev¹, V. Y. Yakovlev², M. G. Sertsu³, O. F. Yakushev⁴, V. M. Krivtsun⁵, V. V. Medvedev^{5,1}, Yu. G. Gladush², I. A. Ostanin², A. Sokolov³, F. Schafers³, and A. G. Nasibulin^{2,6}

1 Moscow Institute of Physics and Technology (State University), Institutskiy pereulok str. 9, Dolgoprudny, Moscow region 141701, Russia

2 Skolkovo Institute of Science and Technology, Nobel str. 3, Moscow, 121205, Russia

3 Helmholtz Zentrum Berlin (BESSY-II), Albert-Einstein-Strasse 15, D-12489 Berlin, Germany

4 P. N. Lebedev Physical Institute of the Russian Academy of Science, Moscow, Russia

5 Institute for Spectroscopy of the Russian Academy of Science, Moscow, Troitsk, Russia

6 Department of Applied Physics, Aalto University, 15100, FI-00076 Aalto, Finland

Abstract

Constant demand of increasing optical resolution motivates technologies like photolithography and microscopy to master the short-wavelength range of $\lambda \sim 1\text{-}10$ nm. High natural radiation absorptance of various materials in this range generates challenges for designing high-performance optical systems. Under these conditions, optical elements composed of freestanding ultra-thin films become crucially important. This paper examines the feasibility of single-walled carbon nanotube (SWCNT) thin films for applications in the short-wavelength optics. Test samples were fabricated using an aerosol chemical vapor deposition method. Synchrotron radiation was used to record transmittance spectra of the samples in the wavelength range from 1 to 20 nm. The measured transmittance exceeds 75% for wavelengths below 20 nm for a 40-nm-thick film, at the operational wavelength of the extreme ultraviolet lithography ($\lambda = 13.5$ nm) the transmittance is 88%. The measured stress-strain curve for the test samples shows that the SWCNT films have rather high ductility unlike fragile films made of conventional condensed-matter materials. We use numerical simulations to demonstrate that the film strain mostly happens by means of nanotubes straightening and slipping past each other without forming of strain localization responsible for fragile behavior. The combination of high radiation transmittance and unique mechanical properties makes the SWCNT-films very promising for applications in the short-wavelength optics, specifically for a fabrication of protective membranes or pellicles for the extreme ultraviolet lithography.

I Introduction

The short-wavelength range including soft X-rays and extreme ultraviolet (EUV) is actively explored nowadays. Important examples of applications utilizing the short-wavelength radiation are 1) microscopy and tomography of cells and larger biological objects in the so-called water-window range [1–4]; 2) fabrication of the next-generation integrated circuits with feature sizes below 10 nm using EUV lithography [5,6]; and 3) optical characterization of nanostructures with coherent diffractive imaging [7,8]. Such applications require efficient high-power and/or high-brightness radiation sources and high-resolution optical systems. The intensive development of the source technologies, including the high harmonic generation [9,10], discharge-produced and laser-produced plasmas [11,12] and free-electron lasers [13–15], responds to the first demand. The development of technologies for fabrication of multilayer Bragg mirrors possessing high reflectance at normal incidence responds to the second demand of the advanced optics [16–18]. It is worth mentioning that the fabrication of the classical refractive lenses is impossible in the spectral range of interest due to the strong absorption of the radiation in all

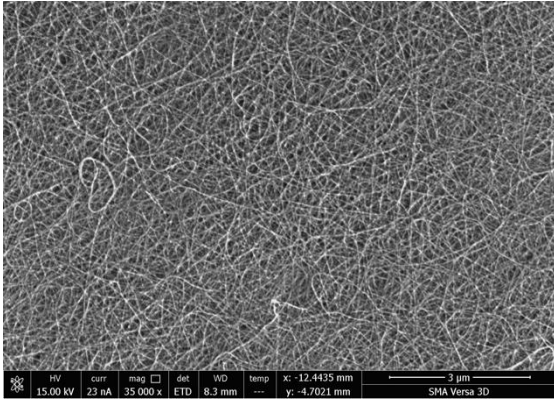
materials without exception. Nevertheless, free-standing films with thicknesses in the range from 10 to 100 nm might demonstrate quite high transmittance. Therefore, such thin films are also of a great importance and scientific interest for the short-wavelength optics.

The free-standing thin films can be used as spectral filters, polarizers or beam-splitters in various optical systems for soft X-rays and EUV radiation [19–29]. The free-standing thin films can also serve as protective membranes or pellicles for the advanced optical elements in order to prevent their contamination with debris particles. The latter application is especially important for the EUV lithography [30,31]. In a lithography process, a pattern on a photomask (reticle) is projected onto a wafer. Contamination of the photomask with particles can cause defects in the printed integrated circuits. In order to avoid the contamination, a pellicle should be mounted in front of the photomask [32,33].

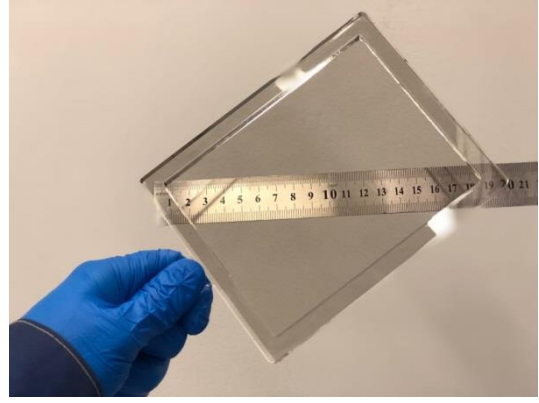
In this paper, we propose a novel material for the short-wavelength optics made of free-standing thin single-walled carbon nanotube (SWCNT) films. The films are prepared by scalable to mass production aerosol CVD synthesis method, which allows film fabrication with lateral sizes of more than 10 cm and thicknesses from 10 to 100 nm. The SWCNT films have the natural difference in their microstructure from that of amorphous and polycrystalline solid films and the concept of brittleness is not applicable to such films. We use a biaxial stretching with a bulge test technique to measure its mechanical properties and perform high performance mesoscale modeling to demonstrate the microscale behavior of the film under deformation. Relatively low absorption cross-sections of carbon atoms at short wavelengths allow achieving high transmittance. For instance, we demonstrate 88% transmittance at the wavelength of 13.5 nm with a 40 nm thick film. In addition to said, a good gas permeability through the structure provides a very attractive set of properties for applications in the short-wavelength optics, e.g. as a strong porous protective membrane.

II Sample fabrication

SWCNTs are synthesized in an aerosol (floating catalyst) CVD reactor described elsewhere [34,35]. Nanotubes grow on aerosol iron nanoparticles floating in the flow of CO atmosphere in a hot wall reactor and then collected on a nitrocellulose filter at the outlet. They form a randomly oriented network (Fig. 1a) consisting of individual SWCNTs and their small bundles. Depending on the collection time it is possible to obtain films of different thicknesses from a few to hundreds of nanometers. SWCNT films can be easily transferred from the filter to various substrates by a dry transfer technique described by Kaskela *et al.* [36]. If the film thickness exceeds 10 nm one can make a large area free-standing films by transferring the SWCNTs on a support frame [37]. All the experimental studies reported below were carried out using 40-nm-thick samples produced with a lab scale reactor and attached to fused silica frames with 5 mm round openings. Nevertheless, the described method can be easily scaled for the fabrication of large area films (e.g. as large as A3 paper size). For instance, Fig. 1b shows a photo of a freestanding SWCNT film with the thickness of 40 nm suspended over a rectangular opening as large as 10x13 cm² that fulfilling the size requirements for the EUV protective pellicles [38].



a)



b)

Fig. 1. a) SEM image of randomly oriented single-walled carbon nanotubes produced by an aerosol CVD synthesis. b) A photograph of a free-standing SWCNT film with the thickness of 40 nm suspended over a rectangular opening with the area of 10x13 cm².

III Optical properties

The short-wavelength transmittance measurements of the samples were performed using s-polarized synchrotron radiation at the facilities of the optics beamline of BESSY-II synchrotron radiation source [39,40]. The normal incident beam spot size which hits the center of the sample was 0.72x0.50 mm². The angular alignments of sample and detector goniometers were tuned with accuracies of ± 0.05 deg. A GaAsP photodetector with an active area of 4x4 mm² was used to accept the direct transmitted rays and most of the scattered parts. The spectral purity of the incident beam from high order diffractions of the monochromator grating was maintained by an efficient high order suppression system installed in the beamline [41].

The measured transmittance spectrum is shown with solid red line in Fig. 2. The transmittance T at the wavelength of 40 nm equals 48 %. One can see that T first increases up to 98.2 % with decreasing wavelength λ and then the transmittance drops at wavelengths just below $\lambda \approx 4.4$ nm, which corresponds to the K photoabsorption edge of carbon. T takes its minimum value of 80.3 % at $\lambda \approx 4.2$ nm and then it increases again with the wavelength decrease.

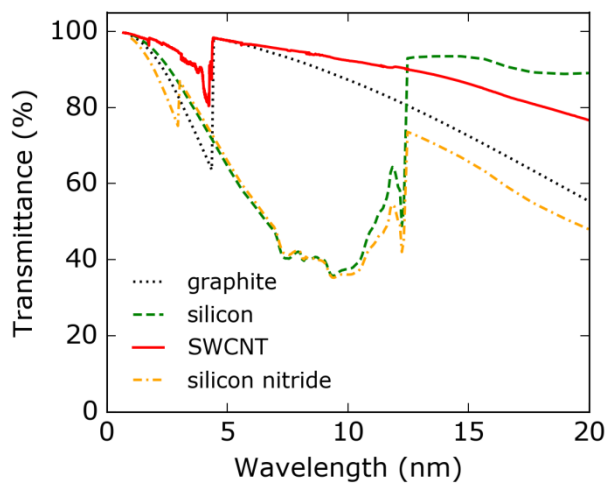


Fig. 2. Experimental transmittance spectrum for a 40-nm-thick film of SWCNTs (solid red line) and calculated transmittance spectra for 40-nm-thick films of silicon (green dot-dashed line), silicon nitride (blue dotted line) and graphite (gray dashed line).

In Fig. 2, we also compare the measured transmittance spectrum for the SWCNTs with calculated transmittance spectra of 40-nm-thick films of silicon, silicon nitride and graphite. Feasibility of the fabrication of ultrathin free-standing films of these materials has been previously demonstrated [42–44]. Transmittance spectra were calculated using the following equation:

$$T = \left| \frac{4n \exp(2\pi i n d / \lambda)}{(1+n)^2 - (1-n)^2 \exp(4\pi i n d / \lambda)} \right|^2, \quad (1)$$

where d denotes the film thickness, λ is the radiation wavelength, n is the complex index of refraction of a given material at the wavelength λ . The values of n for the aforementioned materials were taken from the Henke database. It is seen that the SWCNT films promise higher transmittance than those of silicon nitride and graphite films over the entire considered spectral range. And the SWCNT films promise higher transmittance than that of pure silicon in the range below the L photoabsorption edge of Si, i.e. for $\lambda < 12.4$ nm. Higher transmittance of the SWCNT films compared to graphite is due to lower mass density of the SWCNT films.

IV Mechanical properties

Experimental tests. The bulge test was used to evaluate mechanical properties of the studied SWCNT thin films. In such test, a thin film sample is clamped over an orifice and a uniform gas pressure is applied from one of the film sides. The deflection of the film is then measured as a function of the gas pressure allowing determination of the stress-strain curve. Our experimental setup is schematically shown in Fig. 3. Samples of the SWCNT thin films fixed onto ring-shaped fused silica substrates with 5 mm central opening were used the experiments. Such a sample was hermetically clamped over the orifice dividing the vacuum chamber into two volumes V_1 and V_2 as shown in Fig. 3. These two volumes were also connected by an additional bypass channel with a valve. First, the entire chamber was pumped to the base pressure of $4 \cdot 10^{-5}$ Pa. The pumping was carried out with open bypass valve. Then, with the closed bypass valve, the volume V_1 was filled with argon to a given pressure P_1 , which was controlled by a thermocouple pressure gauge. Pressure in the volume V_2 denoted as P_2 was measured using an ionization vacuum pressure gauge. Note that the pressure differentiation P_2/P_1 was of the order of 10^{-3} in the experiments. Curvature of the film under the pressure load was determined by measured deflection of the reflected laser beam.

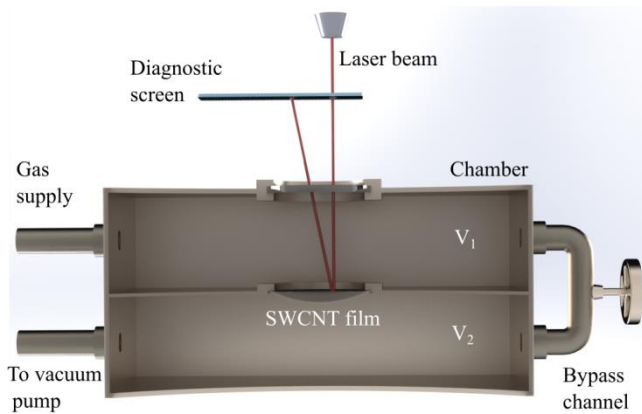


Fig. 3. Scheme of the experimental setup for the bulge test: a free standing film is deformed under gas pressure deflecting the laser beam. Shift of the laser spot on the ruler gives the curvature of the film.

The pressure load $\Delta P = P_1 - P_2$ causes a deformation of the film. For small deformations, the shape of a curved film can be approximated by a sphere. As mentioned above, the radius of curvature R of the deformed film was measured from the angular deflection of the reflected laser beam. In the case of small deformations, the relative stretching of the film can be calculated from the following formula:

$$\varepsilon = \frac{2}{3} \left(\frac{h}{a} \right)^2, \quad (2)$$

where a denotes the radius of the opening on which the film is fixed, $h \approx a^2 / 2R$ is the film deflection in the center. The stress σ arising in the deformed film can be calculated by the following formula:

$$\sigma = \frac{\Delta P R}{2d}, \quad (3)$$

where d denotes the film thickness. It is important to note that Eqs. (2) and (3) are derived on the assumption that in the initial state the surface of the film is flat and it is not stressed. In reality, it is extremely difficult to produce such initial conditions. Most often, as a result of fixing on the holder, the film has non-zero initial stress, or vice versa, it becomes slack.

In these experiments, the SWCNT films were initially slack. To show that, we plot the measured film deflection h as a function of the pressure load (Fig. 4A). It is evident that h remains non-zero upon the application of infinitesimal pressures, i.e. $h = h_0$ at $\Delta P = 0^+$. In this case the equation for the film strain should be corrected as follows:

$$\varepsilon = \frac{2}{3a^2} (h^2 - h_0^2). \quad (4)$$

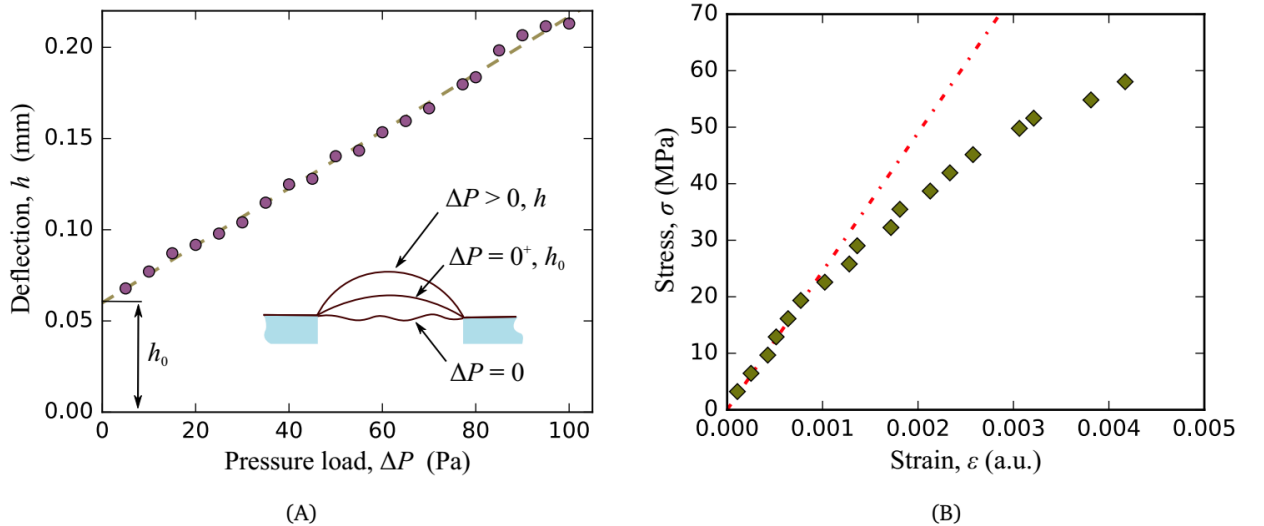


Fig. 4. A) The measured deflection of a 40-nm-thick film as a function of the load pressure in the bulge test. B) The measured stress-strain curve for a SWCNT film with 40 nm thickness. Red dot-dashed line corresponds to the fit of the data in the range of linear deformation with $Y = \sigma/\varepsilon = 24.5$ GPa.

Fig. 4B shows the measured stress-strain curve for the 40-nm-thick SWCNT film. For $\varepsilon < 0.001$, the measured stress is linearly proportional to the strain. Hence, it is possible to define the biaxial modulus Y of the film in this range as $Y = \sigma/\varepsilon$. The measured data gives $Y = 24.5$ GPa. For $\varepsilon > 0.001$, the linear dependence of σ on ε is violated, but the deformation remains elastic up to the yield point of $\varepsilon = 0.003$. The measured stress at $\varepsilon = 0.003$ is $\sigma = 52$ MPa. This stress value corresponds to the experimental gas pressure load of $\Delta P \approx 80$ Pa. In the experiments, the gas pressure was increased until the fracture of the sample occurred. The corresponding pressure was as high as 5.3 kPa. At this point the deformation of the sample was so large that the probe laser beam was deflected beyond the detector aperture. For that reason, it was not possible to measure the corresponding values of strain and stress. However, such a large difference in the pressures corresponding to the yield and fracture points allows to conclude that the studied SWCNT films can be categorized as a very ductile material.

There is a number of publications devoted to the investigation of the mechanical properties of thin freestanding films made of other materials that can be used as a filter of the EUV radiation, e.g. SiN_x , Al and MoSi_2 [46,47]. These publications show that the fracture of such materials occurs on the linear part of the stress-strain curve characterizing such films as extremely brittle. In case of application of freestanding thin films for the protection of EUV optical surfaces from contamination, the ductile SWCNT films can be advantageous over the fragile films made of conventional condensed matter materials. If a brittle film fixed in front of a protected optical element fractures under an accidental excessive mechanical load then its fragments can contaminate the protected optical surface. Contrarily, SWCNT films have a large safety margin associated with a wide range of plastic deformation.

Numerical evaluation. In order to interpret the aforementioned mechanical properties of freestanding SWCNT films, we carried out high-performance numerical simulations of the SWCNT film mechanics. For this purpose we employed a mesoscale modeling technique [48, 49, 50]. It is based on time integration of damped dynamics of chains of rigid cylinders, connected with 3D elastic bonds [51] and interacting via realistic coarse-grained vdW potential, allowing for relative slip of SWCNTs in contact. Molecular dynamics simulations were used for the model calibration.

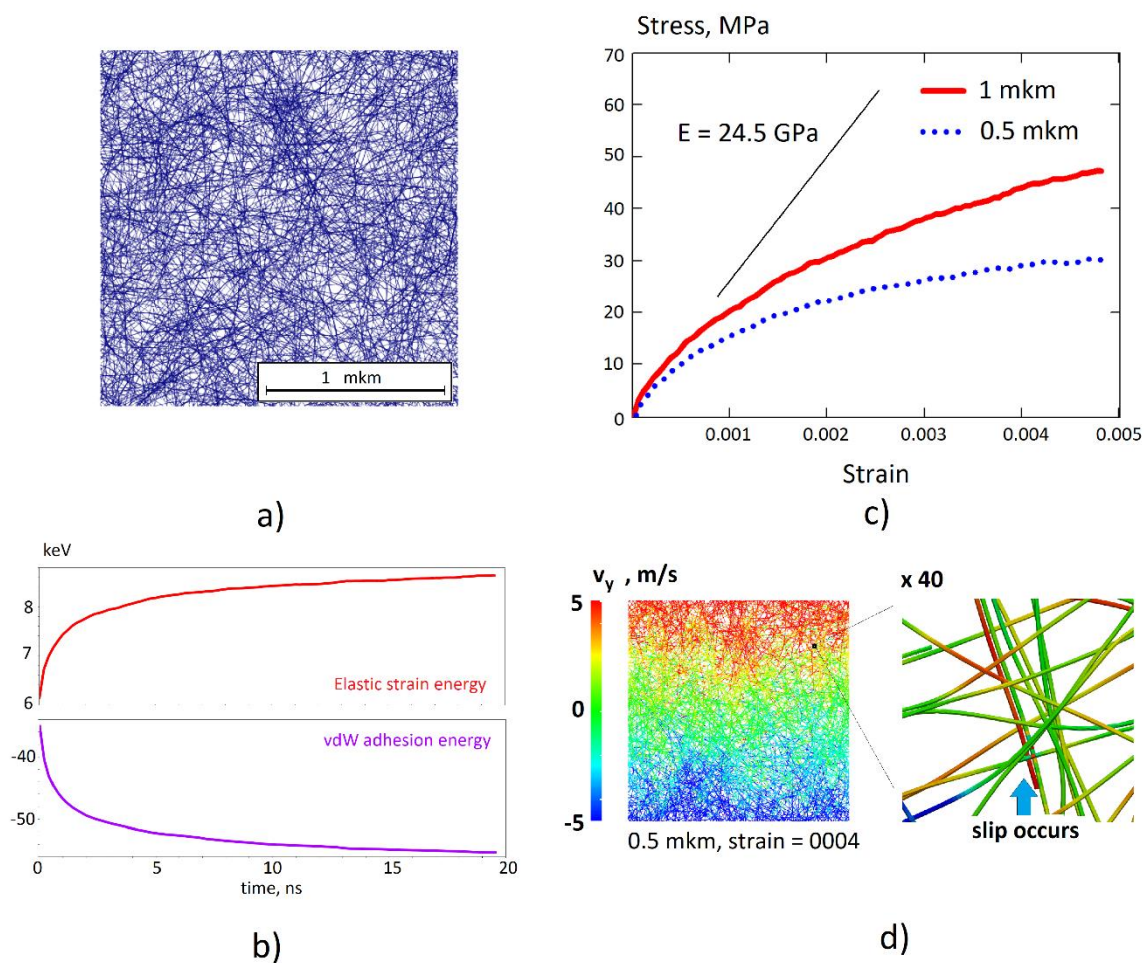


Fig. 6. (A) Specimen of a CNT film and schematics of biaxial mechanical test (B) Evolution of the potential energy terms during the relaxation of a 1 μm SWCNT film specimen. (C) Stress-strain curves observed in a biaxial test (D) Scalar field of vertical velocity component, indicating the slip of separate CNTs during plastic deformation.

We tested a $2 \times 2 \mu\text{m}^2$ SWCNT film specimen, with a density of 0.35 g/cm^3 , the film thickness of 20 nm and periodic boundary conditions in out-of-plane direction (“thick film” approximation). Two specimen sets contained 2000 (10,10) SWCNTs with the length of 0.5 μm and 1000 (10,10) SWCNTs with length of 1 μm . At the initial stage of numerical experiments, straight SWCNTs were deposited in plane with uniform random in-plane orientations and slight out-of-plane deviations, and then relaxed to the energy minimum state, forming a network of interconnected bundles due to the van der Waals (vdW) adhesion (Fig. 6(A)). Equilibration of the SWCNT film structure is characterized by the decrease in vdW adhesion energy due to formation of bundles together with increase in the elastic strain energy due to the bending of SWCNTs (Fig. 6(B)). At the second stage, a biaxial tension load was applied with the rate of deformation sufficiently low to exclude inertial effects, leaving relatively small rate dependence associated with realistic energy dissipation during relative SWCNT slip. Biaxial tension was used to model the free-standing film bulge test described above.

Our numerical simulations have demonstrated results that are in a good qualitative agreement with the experimental data. The stress-strain curve observed (Fig. 6(C)) featured a linear elastic regime and the

initial stage of deformation, followed by a plastic flow. Yielding threshold in the model appeared to be very close to one observed in experiment, approximately 0.1-0.2%. The biaxial moduli (26 GPa for 1 μm SWCNTs and 22 GPa for 0.5 μm SWCNTs) of the film specimens appeared to be close to the one observed in experiment. However, the plastic yield stress was substantially lower. We attribute this difference to a larger SWCNT length and higher degree of bundling of SWCNTs in the film used in the experiment, since the SWCNT bundling occurs not only on the filter during the collection, as was simulated in the calculations, but also in the gas phase after their synthesis before the SWCNTs got collected on a filter.

Our simulations clearly demonstrated that the plastic deformation of SWCNT films observed both in the experiment and simulation is conditioned by a relative slip of SWCNTs in a plane, which is illustrated in Fig. 6(D). The color on the left picture corresponds the SWCNT velocity projection on the y-axis. One can see that SWCNTs closer to the edge have large speed towards stretching direction, however, unlike the bulk materials, velocity field is distributed nonuniformly due to SWCNT straightening and slipping past each other. It is seen more clearly under stronger magnification (right picture) where neighboring SWCNTs have different velocities. Recent computational works [52,53] demonstrate that such slip does not localize due to stabilizing role of energy dissipation and does not lead to significant changes in the structure and properties of the SWCNTs, unless the strain reaches a few tens percent. At strains up to 10% such plastic flow does not lead to localized damage development.

Conclusions

We synthesized SWCNTs by an aerosol CVD method, fabricated freestanding thin films and examined their optical and mechanical properties. The method allows to produce specimens the with lateral sizes of more than 10 cm and thicknesses from 10 to 100 nm making it very attractive for industrial applications. The soft X-ray and EUV transmittance spectra of a 40-nm film was measured using the synchrotron radiation. The measured transmittance at the operational wavelength of EUV lithography was as high as 88%, which meets the demands of various applications. Mechanical properties of the films were characterized by the bulge test. The stress-strain curve of the samples demonstrates high ductility of the SWCNT films, which allows them to withstand high pressure loads. High performance numerical modeling using mesoscale technique was employed to understand the behavior of the film under strain at microscale. We have shown that SWCNT slip is responsible for ductile behavior of the film preventing from brittle failure. The combination of high EUV transmittance and unique mechanical properties of the SWCNT films makes them extremely attractive for applications in EUV optics, and particularly, for fabrication of the protective pellicles for EUV photomask.

Acknowledgements

Mr. Andrei Starkov is acknowledged for the help with drawing of 3D schematics of the experimental setup. The authors (V. Y. Y., Yu. G. G. and A.G.N.) acknowledge Russian Science Foundation (Project identifier: 17-19-01787) for the support of the experimental part of the research. I. O. acknowledges Russian Science Foundation (Project identifier: 17-73-10442) for the support of numerical modeling part of the work. This work was supported by Skoltech NGP Program (Skoltech-MIT joint project). The authors thank CANATU Ltd., a leading company in freestanding nanocarbon films, for providing a large area demonstration sample.

References:

- [1] M. Berglund, L. Rymell, M. Peuker, T. Wilhein, and H. M. Hertz, *J. Microsc.* **197**, 268 (2000).
- [2] W. Chao, B. D. Harteneck, J. A. Liddle, E. H. Anderson, and D. T. Attwood, *Nature* **435**, 1210 (2005).

- [3] M. A. Le Gros, G. McDermott, and C. A. Larabell, *Carbohydr. Glycoconjugates Biophysical Methods* **15**, 593 (2005).
- [4] D. Y. Parkinson, G. McDermott, L. D. Etkin, M. A. Le Gros, and C. A. Larabell, *J. Struct. Biol.* **162**, 380 (2008).
- [5] C. Wagner and N. Harned, *Nat. Photonics* **4**, 24 (2010).
- [6] Jan van Schoot, Eelco van Setten, Gijsbert Rispens, Kars Z. Troost, Bernhard Kneer, Sascha Migura, Jens Timo Neumann, and Winfried Kaiser, **16**, 41010 (2017).
- [7] M. D. Seaberg, B. Zhang, D. F. Gardner, E. R. Shanblatt, M. M. Murnane, H. C. Kapteyn, and D. E. Adams, *Optica* **1**, 39 (2014).
- [8] P. D. Baksh, M. Odstrčil, H.-S. Kim, S. A. Boden, J. G. Frey, and W. S. Brocklesby, *Opt. Lett.* **41**, 1317 (2016).
- [9] T. Popmintchev, M.-C. Chen, A. Bahabad, M. Gerrity, P. Sidorenko, O. Cohen, I. P. Christov, M. M. Murnane, and H. C. Kapteyn, *Proc. Natl. Acad. Sci.* **106**, 10516 (2009).
- [10] T. Popmintchev, M.-C. Chen, D. Popmintchev, P. Arpin, S. Brown, S. Ališauskas, G. Andriukaitis, T. Balčiūnas, O. D. Mücke, A. Pugzlys, A. Baltuška, B. Shim, S. E. Schrauth, A. Gaeta, C. Hernández-García, L. Plaja, A. Becker, A. Jaron-Becker, M. M. Murnane, and H. C. Kapteyn, *Science* **336**, 1287 (2012).
- [11] V Y Banine and K N Koshelev and G H P M Swinkels, *J. Phys. Appl. Phys.* **44**, 253001 (2011).
- [12] Fomenkov Igor, Brandt David, Ershov Alex, Schafgans Alexander, Tao Yezheng, Vaschenko Georgiy, Rokitski Slava, Kats Michael, Vargas Michael, Purvis Michael, Rafac Rob, La Fontaine Bruno, De Dea Silvia, LaForge Andrew, Stewart Jayson, Chang Steven, Graham Matthew, Riggs Daniel, Taylor Ted, Abraham Mathew, and Brown Daniel, *Adv. Opt. Technol.* **6**, 173 (2017).
- [13] W. Ackermann, G. Asova, V. Ayvazyan, A. Azima, N. Baboi, J. Bähr, V. Balandin, B. Beutner, A. Brandt, A. Bolzmann, R. Brinkmann, O. I. Brovko, M. Castellano, P. Castro, L. Catani, E. Chiadroni, S. Choroba, A. Cianchi, J. T. Costello, D. Cubaynes, J. Dardis, W. Decking, H. Delsim-Hashemi, A. Delsérieys, G. Di Pirro, M. Dohlus, S. Düsterer, A. Eckhardt, H. T. Edwards, B. Faatz, J. Feldhaus, K. Flöttmann, J. Frisch, L. Fröhlich, T. Garvey, U. Gensch, C. Gerth, M. Görler, N. Golubeva, H.-J. Grabosch, M. Grecki, O. Grimm, K. Hacker, U. Hahn, J. H. Han, K. Honkavaara, T. Hott, M. Hüning, Y. Ivanisenko, E. Jaeschke, W. Jalmuzna, T. Jezynski, R. Kammering, V. Katalev, K. Kavanagh, E. T. Kennedy, S. Khodyachykh, K. Klose, V. Kocharyan, M. Körfer, M. Kollwe, W. Koprek, S. Korepanov, D. Kostin, M. Krassilnikov, G. Kube, M. Kuhlmann, C. L. S. Lewis, L. Lilje, T. Limberg, D. Lipka, F. Löhl, H. Luna, M. Luong, M. Martins, M. Meyer, P. Michelato, V. Miltchev, W. D. Möller, L. Monaco, W. F. O. Müller, O. Napieralski, O. Napoly, P. Nicolosi, D. Nölle, T. Nuñez, A. Oppelt, C. Pagani, R. Paparella, N. Pchalek, J. Pedregosa-Gutierrez, B. Petersen, B. Petrosyan, G. Petrosyan, L. Petrosyan, J. Pflüger, E. Plönjes, L. Poletto, K. Pozniak, E. Prat, D. Proch, P. Pucyk, P. Radcliffe, H. Redlin, K. Rehlich, M. Richter, M. Roehrs, J. Roensch, R. Romaniuk, M. Ross, J. Rossbach, V. Rybnikov, M. Sachwitz, E. L. Saldin, W. Sandner, H. Schlarb, B. Schmidt, M. Schmitz, P. Schmüser, J. R. Schneider, E. A. Schneidmiller, S. Schnepp, S. Schreiber, M. Seidel, D. Sertore, A. V. Shabunov, C. Simon, S. Simrock, E. Sombrowski, A. A. Sorokin, P. Spanknebel, R. Spesyvtsev, L. Staykov, B. Steffen, F. Stephan, F. Stulle, H. Thom, K. Tiedtke, M. Tischer, S. Toleikis, R. Treusch, D. Trines, I. Tsakov, E. Vogel, T. Weiland, H. Weise, M. Wellhöfer, M. Wendt, I. Will, A. Winter, K. Wittenburg, W. Wurth, P. Yeates, M. V. Yurkov, I. Zagorodnov, and K. Zapfe, *Nat. Photonics* **1**, 336 (2007).
- [14] T. Shintake, H. Tanaka, T. Hara, T. Tanaka, K. Togawa, M. Yabashi, Y. Otake, Y. Asano, T. Bizen, T. Fukui, S. Goto, A. Higashiya, T. Hirono, N. Hosoda, T. Inagaki, S. Inoue, M. Ishii, Y. Kim, H. Kimura, M. Kitamura, T. Kobayashi, H. Maesaka, T. Masuda, S. Matsui, T. Matsushita, X. Maréchal, M. Nagasono, H. Ohashi, T. Ohata, T. Ohshima, K. Onoe, K. Shirasawa, T. Takagi, S. Takahashi, M. Takeuchi, K. Tamasaku, R. Tanaka, Y. Tanaka, T. Tanikawa, T. Togashi, S. Wu, A. Yamashita, K. Yanagida, C. Zhang, H. Kitamura, and T. Ishikawa, *Nat. Photonics* **2**, 555 (2008).
- [15] E. Allaria, R. Appio, L. Badano, W. A. Barletta, S. Bassanese, S. G. Biedron, A. Borga, E. Busetto, D. Castronovo, P. Cinquegrana, S. Cleva, D. Cocco, M. Cornacchia, P. Craievich, I. Cudin, G. D’Auria, M. Dal Forno, M. B. Danailov, R. De Monte, G. De Ninno, P. Delgiusto, A. Demidovich, S. Di Mitri, B. Diviacco, A. Fabris, R. Fabris, W. Fawley, M. Ferianis, E. Ferrari, S. Ferry, L. Froehlich, P. Furlan, G. Gaio, F. Gelmetti, L. Giannessi, M. Giannini, R. Gobessi, R. Ivanov, E. Karantzoulis, M. Lonza, A. Lutman, B. Mahieu, M. Milloch, S. V. Milton, M. Musardo, I. Nikolov, S. Noe, F. Parmigiani, G. Penco, M. Petronio, L. Pivetta, M. Predonzani, F. Rossi, L. Rumiz, A. Salom, C. Scafuri, C. Serpico, P. Sigalotti, S. Spampinati, C. Spezzani, M. Svandrlík, C. Svetina, S.

- Tazzari, M. Trovo, R. Umer, A. Vascotto, M. Veronese, R. Visintini, M. Zaccaria, D. Zangrando, and M. Zangrando, *Nat. Photonics* **6**, 699 (2012).
- [16] E. Louis, A. E. Yakshin, T. Tsarfati, and F. Bijkerk, *Prog. Surf. Sci.* **86**, 255 (2011).
- [17] Mariya M Barysheva and Alexey E Pestov and Nikolai N Salashchenko and Mikhail N Toropov and Nikolai I Chkhalo, *Phys.-Uspekhi* **55**, 681 (2012).
- [18] Q. Huang, V. Medvedev, R. van de Kruijs, A. Yakshin, E. Louis, and F. Bijkerk, *Appl. Phys. Rev.* **4**, 11104 (2017).
- [19] Forbes R. Powell, Peter W. Vedder, Joakim F. Lindblom, and Stephen F. Powell, **29**, 29 (1990).
- [20] F. M. Quinn, D. Teehan, M. MacDonald, S. Downes, and P. Bailey, *J. Synchrotron Radiat.* **5**, 783 (1998).
- [21] J. F. Seely, *Appl. Opt.* **41**, 5979 (2002).
- [22] V. P. Belik, Y. M. Zadiranov, N. D. Il'inskaya, A. V. Korlyakov, V. V. Luchinin, M. A. Markosov, R. P. Seisyan, and É. M. Sher, *Tech. Phys. Lett.* **33**, 508 (2007).
- [23] Masatoshi Hatayama and Hisataka Takenaka and Eric M. Gullikson and Akira Suda and Katsumi Midorikawa, *Jpn. J. Appl. Phys.* **48**, 122202 (2009).
- [24] Nikolay I. Chkhalo, Mikhail N. Drozdov, Evgeniy B. Klunokov, Alexsei Ya. Lopatin, Valerii I. Luchin, Nikolay N. Salashchenko, Nikolay N. Tsybin, Leonid A. Sjmaenok, Vadim E. Banine, and Andrei M. Yakunin, **11**, 21115 (2012).
- [25] E B Klyuenkov and A Ya Lopatin and V I Luchin and Nikolai N Salashchenko and N N Tsybin, *Quantum Electron.* **43**, 388 (2013).
- [26] R. Sobierajski, R. A. Loch, R. W. E. van de Kruijs, E. Louis, G. von Blanckenhagen, E. M. Gullikson, F. Siewert, A. Wawro, and F. Bijkerk, *J. Synchrotron Radiat.* **20**, 249 (2013).
- [27] S. P. Huber, V. V. Medvedev, J. Meyer-Ilse, E. Gullikson, B. Padavala, J. H. Edgar, J. M. Sturm, R. W. E. van de Kruijs, D. Prendergast, and F. Bijkerk, *Opt. Mater. Express* **6**, 3946 (2016).
- [28] N. I. Chkhalo, M. N. Drozdov, E. B. Klunokov, S. V. Kuzin, A. Y. Lopatin, V. I. Luchin, N. N. Salashchenko, N. N. Tsybin, and S. Y. Zuev, *Appl. Opt.* **55**, 4683 (2016).
- [29] J. L. P. Barreaux, I. V. Kozhevnikov, M. Bayraktar, R. W. E. Van De Kruijs, H. M. J. Bastiaens, F. Bijkerk, and K.-J. Boller, *Opt. Express* **25**, 1993 (2017).
- [30] C. Asbach, H. Fissan, J. H. Kim, S.-J. Yook, and D. Y. H. Pui, *J. Nanoparticle Res.* **8**, 705 (2006).
- [31] S. J. Yook, H. Fissan, C. Asbach, J. H. Kim, D. D. Dutcher, P. Y. Yan, and D. Y. H. Pui, *IEEE Trans. Semicond. Manuf.* **20**, 578 (2007).
- [32] Luigi Scaccabarozzi, Dan Smith, Pedro Rizo Diago, Eric Casimiri, Nina Dziomkina, and Henk Meijer, in (2013), pp. 867904-8679-12.
- [33] Brouns Derk, *Adv. Opt. Technol.* **6**, 221 (2017).
- [34] A. Moisala, A. G. Nasibulin, D. P. Brown, H. Jiang, L. Khriachtchev, and E. I. Kauppinen, *John Bridg. Symp. Shap. Future Chem. Eng.* **61**, 4393 (2006).
- [35] Y. Tian, A. G. Nasibulin, B. Aitchison, T. Nikitin, J. v. Pfaler, H. Jiang, Z. Zhu, L. Khriachtchev, D. P. Brown, and E. I. Kauppinen, *J. Phys. Chem. C* **115**, 7309 (2011).
- [36] A. Kaskela, A. G. Nasibulin, M. Y. Timmermans, B. Aitchison, A. Papadimitratos, Y. Tian, Z. Zhu, H. Jiang, D. P. Brown, A. Zakhidov, and E. I. Kauppinen, *Nano Lett.* **10**, 4349 (2010).
- [37] A. G. Nasibulin, A. Kaskela, K. Mustonen, A. S. Anisimov, V. Ruiz, S. Kivistö, S. Rackauskas, M. Y. Timmermans, M. Pudas, B. Aitchison, M. Kauppinen, D. P. Brown, O. G. Okhotnikov, and E. I. Kauppinen, *ACS Nano* **5**, 3214 (2011).
- [38] Image taken with free-standing SWCNT film, produced by CANATU Oy (<https://canatu.com/>) with the identical method discussed in the paper.
- [39] F. Schäfers, P. Bischoff, F. Eggenstein, A. Erko, A. Gaupp, S. Künstner, M. Mast, J.-S. Schmidt, F. Senf, F. Siewert, A. Sokolov, and T. Zeschke, *J. Synchrotron Radiat.* **23**, 67 (2016).
- [40] A. Sokolov, P. Bischoff, F. Eggenstein, A. Erko, A. Gaupp, S. Künstner, M. Mast, J.-S. Schmidt, F. Senf, F. Siewert, T. Zeschke, and F. Schäfers, *Rev. Sci. Instrum.* **87**, 52005 (2016).
- [41] A. Sokolov, M. G. Sertsu, A. Gaupp, M. Lüttecke, and F. Schäfers, *J. Synchrotron Radiat.* **25**, 100 (2017).
- [42] S.-G. Kim, D.-W. Shin, T. Kim, S. Kim, J. H. Lee, C. G. Lee, C.-W. Yang, S. Lee, S. J. Cho, H. C. Jeon, M. J. Kim, B.-G. Kim, and J.-B. Yoo, *Nanoscale* **7**, 14608 (2015).
- [43] Dario L. Goldfarb, in (2015), p. 96350A-9635-13.
- [44] P. J. van Zwol, M. Nasalevich, W. P. Voorthuijzen, E. Kurganova, A. Notenboom, D. Vles, M. Peter, W. Symens, A. J. M. Giesbers, J. H. Klootwijk, R. W. E. van de Kruijs, and W. J. van der Zande, in (2017), p. 1045100-10451-9.

- [45] C. K. Huang, W. M. Lou, C. J. Tsai, T.-C. Wu, and H.-Y. Lin, *Thin Solid Films* **515**, 7222 (2007).
- [46] G. F. Cardinale and R. W. Tustison, *Thin Solid Films* **207**, 126 (1992).
- [47] N. I. Chkhalo, S. V. Kuzin, A. Y. Lopatin, V. I. Luchin, N. N. Salashchenko, S. Y. Zuev, and N. N. Tsybin, *Thin Solid Films* **653**, 359 (2018).
- [48] I. Ostanin, R. Ballarini, D. Potyondy and T. Dumitrica. *Journ. Mech. Phys. Sol.* **61** (3), 762-782(2013).
- [49] I.Ostanin, R.Ballarini, T.Dumitrica. *Journ.Appl.Mech.*, 81 / 061004, pp.1-9, 2014.
- [50] I. Ostanin, P. Zhilyaev, V. Petrov, T. Dumitrica, S. Eibl, U. Ruede, V. Kuzkin. *Letters on Materials* **8**(3) 240-245(2018).
- [51] V. Kuzkin, I. Asonov. *Phys. Rev. E*, **86**(5), 051301(2012).
- [52] Y. Wang, G. Drozdov, E. Hobbie, T. Dumitrica. *ACS Appl. Mat. Int.* 9 (15), 13611-13618(2017).
- [53] Y. Wang, H.Xu G. Drozdov T. Dumitrica. *Carbon*, **139**, 94-104(2018).